The Rocklea Dome 3D Mineral Mapping Test Data Set

Carsten Laukamp[a], Maarten Haest[b], Thomas Cudahy[c]

[a]*CSIRO Mineral Resources, 26 Dick Perry Avenue, Kensington, WA 6151, Australia*

(corresponding author: Carsten.Laukamp@csiro.au)

[b]*MineSense Technologies, Vancouver, Canada*

[c]*C3DMM Pty Ltd, Perth, Australia*

ABSTRACT

The integration of surface and subsurface geoscience data is critical for efficient and effective mineral exploration and mining. Publicly accessible datasets to evaluate the various geoscience analytical tools and their effectiveness for characterisation of mineral assemblages and lithologies or discrimination of ore from waste are however scarce. The open access Rocklea Dome 3D Mineral Mapping Test Data Set (Laukamp, 2020; https://doi.org/10.25919/5ed83bf55be6a) provides an opportunity for evaluating proximal and remote sensing data, validated and calibrated by independent geochemical and mineralogical analyses, for exploration of channel-iron deposits (CID) through cover. We present hyperspectral airborne, surface and drill core reflectance spectra collected in the visible-near infrared and shortwave infrared wavelength ranges (VNIR-SWIR; 350 to 2,500 nm), as well as whole rock geochemistry obtained by means of X-Ray fluorescence analysis and loss on ignition measurements of drill core samples.

The integration of surface with subsurface hyperspectral data collected in the frame of previously published Rocklea Dome 3D Mineral Mapping case studies demonstrated that about 30% of exploration drill holes were sunk into barren ground and could have been of better use, located elsewhere, if airborne hyperspectral imagery had been consulted for drill hole planning. The remote mapping of transported Tertiary detritals (i.e. potential hosts of channel iron ore

28   resources) versus weathered in situ Archaean ~~geology~~ bedrock (i.e. barren ground) has

29   significant implications for other areas where "cover" (i.e. regolith and/or sediments covering

30   bedrock hosting mineral deposits) hinders mineral exploration. Hyperspectral remote sensing

31   represents a cost-effective method for regolith landform mapping required for planning drilling

32   programs. In the Rocklea Dome area, vegetation unmixing methods applied to airborne

33   hyperspectral data, integrated with subsurface data, resulted in seamless mapping of ore zones

34   from the weathered surface to the base of the CID – a concept that can be applied to other

35   mineral exploration and mineral deposit studies. Furthermore, the associated, independent

36   calibration data allowed to quantify iron oxide phases and associated mineralogy from

37   hyperspectral data. Using the Rocklea Dome data set, novel geostatistical clustering methods

38   were applied to the drill core data sets for ore body domaining that introduced scientific rigour

39   to a traditionally subjective procedure, resulting in reproducible objective domains that are

40   critical for the mining process.

41   Beyond the already published case studies, the Rocklea Dome 3D Mineral Mapping

42   Test Data Set has the potential to develop new methods for advanced resource characterisation

43   and develop new applications that aid exploration for mineral deposits through cover. The here

44   newly presented white mica and chlorite abundance maps derived from airborne hyperspectral

45   highlight the additional applications of remote sensing for geological mapping and could help

46   to evaluate newly launched hyper- and multispectral spaceborne systems for geoscience and

47   mineral exploration.

48

49   **Key words**: Channel Iron ore Deposits, regolith, hyperspectral remote sensing, hyperspectral

50   drill core sensing, geochemistry

1. INTRODUCTION

The three dimensional (3D) geologic case history of the Rocklea Dome located in the Hamersley Province (Western Australia) targeted the use of reflectance and emission spectroscopy for measuring mineralogy and geochemistry specific to the exploration and characterisation of economic Tertiary channel iron ore deposits in a terrain obscured by weathered, transported materials. This public case history was generated by CSIRO's Western Australian Centre of Excellence for 3D Mineral Mapping (C3DMM), which was operated from 2009 to 2012 and had the primary aim of generating and demonstrating the capabilities for "scalable" 3D mineral mapping from the continental to the prospect scales (Cudahy, 2016). The Rocklea Dome project was established in collaboration with Murchison Metal Ltd, who granted C3DMM access to their drill hole dataset, consisting of 14 diamond cores and 180 reverse circulation drill holes. These drill holes were designed using traditional exploration mapping technologies, such as published geology maps and geophysical data (magnetics and radiometrics).

Key achievements of the Rocklea Dome 3D Mineral Mapping case study include:

- Based on the kaolin crystallinity index derived from surface and sub-surface hyperspectral data (Cudahy, 2016), drill holes were identified that were sunk at surface into barren (i.e. bedrock) weathered material. If surface mineral mapping data, such as airborne hyperspectral imagery, would have been used during drill hole planning, ~~That is,~~ approximately one third of the drill holes need not have been drilled or would have been located differently ~~had surface mineral mapping data, e.g. airborne hyperspectral imagery, been used during drill hole planning~~. This represents potential significant savings in time, money and environmental disturbance.

- Characterisation of clay mineralogy associated with distinct domains of the CID and its cover (i.e. kaolin group vs. Al-smectites vs. Fe-smectites) suggested that clay mineral assemblages as well as calcrete atop buried CIDs have a different composition when compared to regolith covering adjacent areas. That could represent useful information when exploring for CIDs through regolith cover.

- Quantification of iron oxide phases and associated mineralogy derived from hyperspectral data and validated using X-ray diffractometry and geochemistry (Haest et al., 2012 a,b):
  - iron (oxyhydr-)oxide content: RMSE of 9.1 weight % Fe
  - Al clay content: RMSE 3.9 weight % Al_2O_3
  - hematite/goethite ratio: RMSE 9.0 weight % goethite
  - spatial characterisation of vitreous vs. ochreous goethite

- Geological modelling the iron ore resource of the Rocklea Dome CID (Haest et al., 2012 a,b; Cudahy, 2016; Fouedjio et al., 2018), which was reported by Dragon Resources in 2012 to be 72.6Mt (at 53% Fe cut-off) with 54.4% Fe, 7.2% SiO_2, 2.7% Al_2O_3, 0.031% P and 11.2% LOI.

- Improvement of quality of mineral maps by application of vegetation unmixing methods (Haest et al, 2013), resulting in seamless mapping of ore zones from the weathered surface to the base of deposit (Cudahy, 2016).

All the above points showcase how hyperspectral data can be used for critical parts of the mining cycle, especially exploration and 3D resource characterisation.

This article aims to provide an overview of the publicly available hyperspectral data set of the Rocklea Dome, which ought to be used as a test data set for 1) data mining for exploration and mining, 2) integration of independent geoscience data sets (i.e. hyperspectral,

99 geochemical), 3) resource modelling, and 4) different approaches for routine processing of

100 hyperspectral data.

101   The geological setting of the Rocklea Dome area, as well as analytical and processing

102 methods will be discussed first, after which the publicly available test data are listed as a table.

103 Example applications of the geochemical and mineralogical data for exploration, 3D mineral

104 mapping and Resource estimation are summarised briefly in the discussion.

105

106 **2. GEOLOGICAL SETTING**

107

108   The Rocklea Dome Channel Iron Deposit is located in the Hamersley Province, which

109 is the dominant source of Australia's iron ore exports. Channel Iron Deposits (CID) are

110 economically significant formations, providing a substantial percentage of the iron ore mined

111 in Australia. A detailed overview of the geology of the Rocklea Dome and the formation of the

112 CID was provided by Haest et al. (2012b) and is briefly summarised here. The bedrock geology

113 of the Rocklea Dome comprises a monzogranite pluton and cross-cutting mafic and ultramafic

114 intrusives that form part of the Pilbara Craton. The Archean age pluton is overlain by Archaean

115 to Proterozoic metasedimentary and volcanic rocks of the Hamersley Basin, enveloping the

116 central monzogranite dome (Fig. 1; Thorne & Tyler, 1996). Folding is attributed to

117 development of both the Ophthalmia and the Ashburton Fold Belt (Thorne & Tyler, 1996).

118   A meandering Tertiary palaeochannel passes over the Archean and Proterozoic rocks,

119 containing locally Channel Iron ore Deposits (CID), such as the Beasley River CID, which

120 crosscuts the north-western part of the Rocklea Dome. Channel iron ore was also drilled along

121 8 km strike length of a palaeochannel on the eastern side of the Rocklea Dome, which was

122 described by Haest et al. (2012a,b; 2013) as the Rocklea Dome CID (Figure 1). The bedrocks

123 and Tertiary channel are covered partly by regolith (e.g. Quaternary alluvium). Green

124 vegetation and dry vegetation (mostly Spinifex grass and bushes) cover the area partly.

125 A mixture of Fe-Ox pelletoids and ferruginised wood fragments below 10 mm in size

126 represent the major components of CIDs (Morris & Ramanaidou, 2007). In CID systems, the

127 base of the paleochannel often consists of a clay horizon of variable composition. The CID is

128 capped in places by calcrete and silcrete.

129
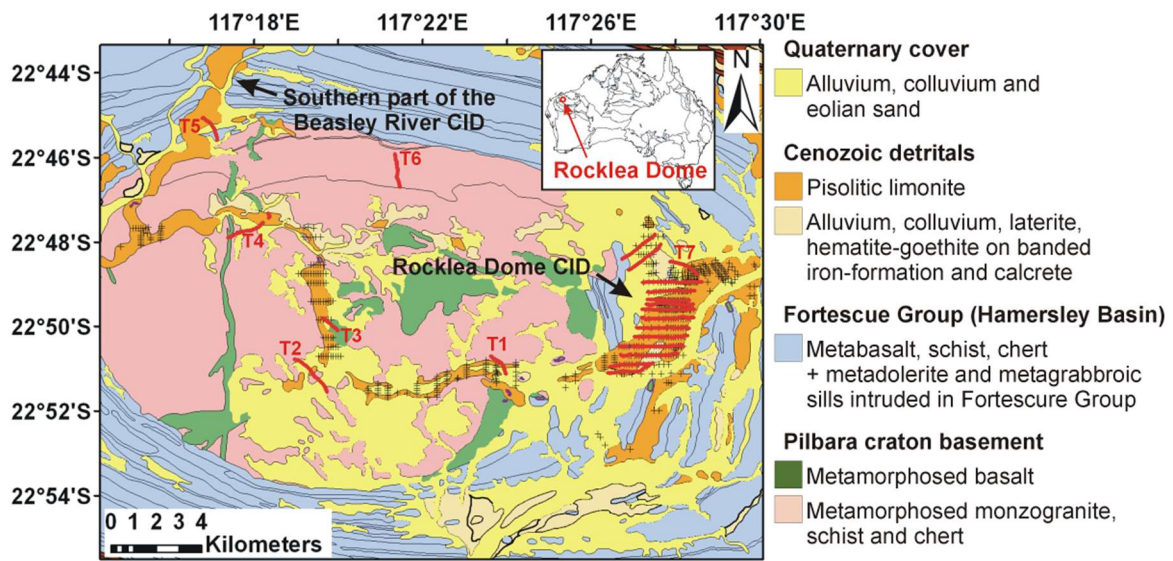
130

131 Figure 1: Geological map of the core of the Rocklea Dome (Haest et al., 2013; Thorne and
132 Tyler, 1996). Validation transects are indicated as red lines. T1 to T7 refer to transects
133 described in Haest et al. (2012a). The black crosses identify the position of all reverse
134 circulation drill cores intersecting the palaeochannel (i.e. pisolitic limonite in map) in the core
135 of the Rocklea Dome.

136

3. METHODS AND MATERIALS

3.1. VNIR-SWIR drill core spectroscopy

Reflectance spectra of 180 rock chips (RC) and 14 diamond drill cores (RKD) were measured using CSIRO's HyChips™ system (cf. Huntington et al., 2004), which comprises a TerraSpec™-based spectrometer (Malvern-Panalytical) system. In total, 7,520 reflectance spectra were collected from RC samples and 66,853 reflectance spectra were collected from RKD samples (Haest et al., 2012a). An automated X-Y table moves the drill core tray in a snake-like pattern below the TerraSpec optical fibre at a distance of ~6 to 13 cm (depending on sample type, i.e., diamond core or drill chips), while the spectral data are collected. Each sample spectrum is collected from a 1 × 1 cm area. Four light globes are positioned 40 cm above and at a small angle (off the backscatter/specular angle) to the measurement/sample point. In addition to hyperspectral data, high spatial resolution (0.1 mm pixel) images are collected from the core or chip tray and the sample height in the tray is measured using a laser profilometer. Reflectance spectra were calibrated using a Teflon/Spectralon™ panel (see Haest et al., 2012a for more details). TerraSpec™ spectra were collected in the visible to near-infrared (VNIR: 380−1,000 nm) and shortwave-infrared (SWIR: 1,000−2,500 nm), with sampling intervals of 1.4 nm in the VNIR and 2.0 nm in the SWIR and a wavelength accuracy of ±1 nm. The spectral resolution is 5 nm in the VNIR and between 11 and 12 nm in the SWIR. The TerraSpec™ radiance spectra of each sample are first converted to apparent bidirectional reflectance using the Teflon signal, which is collected at the beginning/end of each drill core/drill chip tray measurement cycle. This signal is then converted to absolute reflectance, based on the measurement of a Spectralon panel.

3.2. Remote Sensing

7

162   Airborne VNIR–SWIR imagery was collected using the Airborne Multispectral

163   Scanner (AMS), which is an earlier version of HyVista Corporation's HyMap™ system (Cocks

164   et al., 1998). The AMS system collects 96 bands over the VNIR-SWIR, excluding the

165   atmospheric bands from ~1,000 nm to ~1,400 nm and from ~1,800 to ~1,950 nm, respectively.

166   For each spectral band, the average spacing of collected bands is 15 nm and the average full

167   width at half maximum is 17 nm. The AMS data over Rocklea Dome were collected in a north–

168   south direction between the 31st of July 2000 and the 2nd of August 2000, comprising a set of

169   14 flight lines, totalling in a combined length of ~280 km at a pixel size of approximately 7 m.

170   Atmospheric correction was done using MODTRAN5 (Berk et al., 2004, 2006) and SODA

171   (Rodger, 2011), based on a combination of the AMS at-sensor radiance with in-scene flight

172   parameters (e.g. latitude, longitude, sensor height, etc.). For more details about georeferencing

173   and mosaicking the single flight lines, see Haest et al. (2013).

174

175   *3.3.   X-ray fluorescence analysis (XRF)*

176   XRF analysis of 11,900 RC samples (1m interval) for weight percentages of Fe, P, S,

177   SiO_2, Al_2O_3, Mn, CaO, K_2O, MgO, and TiO_2 was conducted by Kalassay Ltd. (now Bureau

178   Veritas Minerals Pty Ltd., Western Australia). A Bruker Pioneer X-ray fluorescence instrument

179   with an end window 4 kW rhodium X-ray tube was used. Sample preparation included drying

180   at 105°C for 12 hr or for 1 hr, depending on whether the sample was wet or dry, respectively.

181   Samples were then crushed to a nominal 90% passing 75 μm. The sample powders were fused

182   in a Herzog automated (RF ~~energized~~energised) fusion furnace and cast into 40 mm diameter

183   beads using a 12:22 flux containing 5% sodium nitrate. Matrix corrections were applied using

184   a calculated alpha correction for this combination of flux, tube, and instrument geometry.

185   Previously determined weight ranges were used for both the sample and the flux weight.

186   Kalassay Ltd. used lab duplicates, internationally certified reference materials, and reference

187 materials of the same ore type as standards and reported a precision better than 0.01% for all

188 analyses. In order to evaluate the accuracy of XRF analyses undertaken by Kalassay Ltd.,

189 duplicate samples were also sent to the Amdel laboratory in Cannington (Western Australia),

190 with good correlation observed (Haest et al., 2012a).

191

192 *3.4. Loss on ignition (LOI)*

193 In order to characterise the mineral assemblages present in the samples in more detail,

194 loss on ignition (i.e., LOI) measurements were undertaken on 11,900 RC samples to record the

195 mass loss of samples on heating (Haest et al., 2012a). A pre-dried portion of all samples was

196 heated in an electric furnace to 1,000°C. During this process, goethite ~~will~~ releases its strongly

197 bonded water and its OH groups between 260°C and 425°C (Strezov et al., 2010), organic

198 matter ~~will be~~ completely ignite~~s~~d by 550°C (Dean, 1974), aluminosilicate clay materials ~~will~~

199 decompose between 530°C and 605°C (Strezov et al., 2010), and inorganic carbon ~~will be~~

200 ~~oxidized~~ is oxidised and lost as CO_2 between 700°C and 850°C (Dean, 1974).

201

202 *3.5. Sample storage*

203 Drill core trays, field samples and XRF standards are all stored at the Australian

204 Resources Research Centre (ARRC) in Kensington (Western Australia). Samples can be

205 viewed and investigated at the ARRC, using local analytical facilities.

206

207 **4. SOFTWARE AND PROCESSING METHODS**

208 *4.1. Processing of hyperspectral drill core data*

209 Hyperspectral drill core data were analysed using the CSIRO's The Spectral Geologist

210 software (TSG^{TM}) by interpreting the abundance, composition and/or crystallinity of selected

211   mineral groups and species using the Multiple Feature Extraction Method. A list of scripts

212   applied to the hyperspectral drill core and rock chip data can be found in Table 1.

Table 1: Base scripts and multiple feature extraction method scripts used for the Rocklea Dome

3D Mineral Mapping project (R = reflectance value at given wavelength).

Product name	Minerals detected	Base algorithm	Filters/Masks	Lower stretch limit	Upper stretch limit (only applicable for composition products)	related publication
Ferric oxide abundance (Ferric_oxide_abundance.txt)	Hematite, goethite, jarosite, "limonite"	Continuum removed depth of the 900 nm absorption calculated using a fitted 2nd order polynomial between 776 and 1,050 nm 900D	R450 > R1650	0.04: low content		further developed on the basis of Haest et al. (2012a,b), which used a 4th order polynomial or 4 band ratio approach
Hematite-goethite distribution (Hematite-goethite_distr.txt)	Hematite-goethite ratio (Cudahy and Ramanaidou, 1997)	Continuum removed wavelength of the 900 nm absorption calculated using a fitted 2nd order polynomial between 776 and 1,050 nm. 900W	R450 > R1650 + 900D >0.025	~890 nm: more hematitic	~910 nm: more goethitic	further developed on the basis of Haest et al. (2012a,b), which used a 4th order polynomial or 4 band ratio approach
Ferrous iron abundance (Ferrous_iron abundance.txt)	Fe^{2+} in silicates & carbonates. (Fe-chlorites, Fe-amphibole, Fe-pyroxene, Fe-olivine, Fe-carbonate)	(R920+R1650)/(R1020+R1235) Ferrous		~1.005: low content		Laukamp et al. (2012)
opaques2 (opaques2inv.txt)	"Reduced" materials such as carbon black, sulphides and magnetite as well as Mn oxides.	albedo @ 1,650 nm 1650	OPAQUES_450D1650 >0.25; albedo @ 1650 nm 1650 <30%	2: low content		
White mica and Al-smectite abundance (wmAlsmai.txt)	Abundance of white micas (e.g. illite, muscovite, paragonite, brammalite, phengite, lepidolite, margarite) and Al-smectites (montmorillonite, beidellite)	Relative absorption depth of the 2,200 nm absorption for which the continuum is removed between 2,120 and 2,245 nm, determined using a 3 band polynomial fit around the band with the lowest reflectance. 2200D	((R2138+R2190)/((R2156 +R2179) 2160D2190 <1.063	0.02: low content		further developed on the basis of Sonntag et al. (2012), which used a 4th order polynomial or 4 band ratio approach
White mica and Al-smectite composition (wmAlsmci.txt)	Tschermak substitution of white micas, ranging from paragonite, brammalite, to illite, muscovite to phengite, and Al-smectites, ranging from beidellite to montmorillonite.	Minimum wavelength of the 2,200 nm absorption for which the continuum is removed between 2,120 and 2,245 nm, determined using a 3 band polynomial fit around the band with the lowest reflectance. 2200W	((R2138+R2190)/(R2156 +R2179) 2160D2190 <1.063	2,180 nm: Al-rich mica (muscovite, illite, paragonite, brammalite, lepidolite)	2,220 nm: Al-poor mica (~phengite)	further developed on the basis of Sonntag et al. (2012), which used a 4th order polynomial or 4 band ratio approach
Kaolin abundance index	Kaolin group minerals, namely kaolinite halloysite, dickite and nacrite	2200D (Normalized depth of a fitted 4th order polynomial between 2,120 and 2,245 nm)	2160D((R2138+R2190)/((R2156+R2179))>1.005	0.02: low content		Sonntag et al. (2012), Haest et al. (2012a,b)
Kaolin composition index	Composition and crystallinity of kaolin group minerals ranging from well-ordered kaolinite to halloysite to dickite (and nacrite)	((R2138+R2173)/R2156)/[(R2156+R2190)/R2173]	2200D=0.005	low values = low crystallinity	high values = high crystallinity	Sonntag et al. (2012), Haest et al. (2012a,b)
Carbonates abundance (carbai3pfit.txt)	carbonates vs. MgOH-bearing silicates, based on left-asymmetry of CO3 feature @ 2,340 nm	Relative absorption depth of the 2340 nm absorption for which the continuum is removed between 2,270 and 2,370, determined using a 3 band polynomial fit around the band with the lowest reflectance. 2340D	2340D>0.04, 2295nm<2340W<2360nm, 2250D < 0.025, 2380D<0.1117*2340D+0.0002, Asymmetry of the 2340 absorption using a fitted 4th order polynomial between 2120 and 2370: 2340 left asym> 1.13	0.05: low content		further developed on the basis of Sonntag et al. (2012), which used a 4th order polynomial or 4 band ratio approach
Carbonate composition (carbci3pfit.txt)	separating calcite, dolomite, siderite, …	Minimum wavelength of the 2,340 nm absorption for which the continuum is removed between 2,270 and 2,370 nm, determined using a 3 band polynomial fit around the band with the lowest reflectance. 2340W	2340D>0.04, 2295nm<2340W<2360nm, 2250D < 0.025, 2380D<0.1117*2340D+0.0002, Asymmetry of the 2340 absorption using a fitted 4th order polynomial between 2120 and 2370: 2340 left asym> 1.13	2,303 nm: magnesite; 2,326 nm: dolomite	2,343 nm: calcite	further developed on the basis of Sonntag et al. (2012), which used a 4th order polynomial or 4 band ratio approach
White mica (+Al-smectite) abundance, refined for airborne hyperspectral imagery	Abundance of white micas (e.g. illite, muscovite, paragonite, brammalite, phengite, lepidolite, margarite) and Al-smectites (montmorillonite, beidellite)	Relative absorption depth of the 2,200 nm absorption for which the continuum is removed between 2,120 and 2,245 nm, determined using a 3 band polynomial fit around the band with the lowest reflectance. 2200D	((R2138+R2190)/((R2156 +R2179) 2160D2190 <1, 2200D/2320D > 1.5	0.04: low content	0.255: high content	further developed on the basis of Sonntag et al. (2012), which used a 4th order polynomial or 4 band ratio approach
Chlorite (+epidote, +biotite) abundance, refined for airborne hyperspectral imagery	Abundance of chlorite (e.g. clinochlore, chamosite), as well as members of the epidote and biotite mineral groups	(R2227+R2275)/(R2241+R2259). 2250D	2250D > 1.01, & 2300 <2320W <2342 & 2240 <2250W < 2260	1.01: low content	1.04: high content	further developed on the basis of Sonntag et al. (2012)

216

4.2.   Image Processing

      The processing strategy for generating geoscience products from AMS data, such as the Kaolin Crystallinity (Table 1) builds on the quality control of the acquired data (Cudahy et al., 2008). Well calibrated radiance-at-sensor or surface reflectance data are required for the processing of airborne hyperspectral imagery. Commonly applied levelling and statistics-based methods were avoided as these introduce undesirable scene-dependencies, making a comparison of image products from different areas impossible. Physics-based reduction models were applied to the remote sensing data, using the image processing software ENVI^{TM}. Complicating effects were removed in their order of development (i.e. 1. instrument, 2. atmospheric, 3. surface effects) through either normalization or offsets.

4.3.   The Multiple Feature Extraction Method

      In hyperspectral proximal (e.g. HyLogging^{TM}) and remote (e.g. AMS) sensing technologies, the VNIR, SWIR, and thermal infrared (TIR: ca. 6,000 – 14,500 nm) wavelength ranges are used to infer abundance and composition of various rocks and minerals in a wide range of sample types, including drill core, rock chips and pulpsgeological materials. The relative intensity and wavelength position of absorption features in the reflectance spectra relate to the physicochemical characteristics of the various minerals. Feature extraction methods can be used to determine the mineralogy of a sample material (Cudahy et al., 2008). The advantage of the multiple feature extraction method (MFEM) is that the associated scripts are not biased on a training dataset or spectral reference libraries, but are based only on the visible and/or infrared active functional groups of minerals (see Laukamp et al., 2011, for more details). As they are instrument independent, the same scripts can be applied to remote sensing and proximal hyperspectral data, easing the integration of, for example, surface (e.g. HyMap)

241 and subsurface data (e.g. HyLogging^{TM}) for the purpose of visualisation in 3D or advanced

242 data analytics. Interferences of mineralogical information with other surface materials such as

243 vegetation can be evaluated by using a multiple linear regression model for unmixing

244 vegetation from hyperspectral remote sensing data (Rodger & Cudahy, 2009; Haest et al.,

245 2013). Other complications, such as spectrally overlapping materials, are removed by the

246 application of thresholds.

247

248 **5. DATA PRODUCTS AND APPLICATIONS**

249 Publicly accessible data of the Rocklea Dome 3D Mineral Mapping project can be

250 found on CSIRO's Data Access Portal:

251 https://data.csiro.au/collections/#collection/CIcsiro:44783

252 (https://doi.org/10.25919/5ed83bf55be6a) and are listed in Table 2. Data and other content on

253 this site are scientific research data collected by CSIRO and third parties and are made available

254 on an 'as is' basis. If any data or other material are downloaded from this site, the user does so

255 at own risk and acknowledges that such data or other content: 1) may contain general

256 statements based on scientific research and may be incomplete and not applicable to all

257 situations; 2) is not professional, scientific, medical, technical or expert advice and is subject

258 to the usual uncertainties of scientific and technical research; and 3) should not be relied upon

259 as specific to you and therefore as the basis for doing or failing to do something. Expert

260 professional scientific and technical advice should be sought prior to acting in reliance on data

261 and other material from this site. To the extent permitted by law, CSIRO excludes all liability

262 to any person for any consequences, including but not limited to all losses, damages, costs,

263 expenses and any other compensation, arising directly or indirectly from using and any

264 information or material contained in it.

265

266 Table 2: Publicly accessible data of the Rocklea Dome 3D Mineral Mapping project

267 (https://data.csiro.au/collections/#collection/CIcsiro:44783;

268 https://doi.org/10.25919/5ed83bf55be6a)

main directory	sub directory	file name	type of data	source/IP
DTM		DTM_Rocklea_50k.00t	Digital terrain model	GSWA
		DTM_Rocklea_50k.dxf		
		DTM_Rocklea_50k.evf		
		DTM_Rocklea_50k.zip		
		Hardey_HR_DTM.00t	Digital terrain model of 100K mapsheet Hardey 2252	GSWA
		Hardey_HR_DTM.dxf		
		Hardey_HR_DTM.evf		
		Topography_ENVI	Digital elevation model	GSWA
		Topography_ENVI.hdr		
		dem_plus_collars.csv	Digital elevation model	GSWA
drill hole data	RC_hyperspectral_geochem	GeoscienceProductDescriptions_ProximalHyperspectral.xlsx	table describing multiple feature extraction scripts applied to hyperspectral data for interpretation of mineralogy	CSIRO
		RC_data.tsg	TSG-file	CSIRO
		RC_data.ini	TSG-file	CSIRO
		RC_data.bip	TSG-file	CSIRO
		RC_data_cras.bip	TSG-file	CSIRO
		RC_data_tsgexport.CSV	spectral and geochemical data exported from TSG	CSIRO
	RKD	RKD5-7-9.tsg	TSG-file	CSIRO
		RKD5-7-9.ini	TSG-file	CSIRO
		RKD5-7-9.bip	TSG-file	CSIRO
		RKD5-7-9_cras.bip	TSG-file	CSIRO
remote sensing data	GeoTIFF_AMS/	2200D_Mstd.tfw	AMS product "2200D", showing the relative abundance of Al-clays	CSIRO
		2200D_Mstd.tif		CSIRO
		2200WAR_2190-2205.tfw	AMS product "2200W", indicating compositional changes of Al-smectites and white micas ($Al^{VI}Al^{IV}(Fe,Mg)_{-1}Si_{-1}$)	CSIRO
		2200WAR_2190-2205.tif		CSIRO
		2250_MStd.tfw	AMS product "2250D", showing the relative abundance of chlorite, epidote and/or biotite	CSIRO
		2250_MStd.tif		CSIRO
		2330_2250-2380.tfw	AMS product "Carbonate abundance", showing the relative abundance of carbonates	CSIRO
		2330_2250-2380.tif		CSIRO
		KC_NoSM_22D+216DM_3MeFi.tfw	AMS product "Kaolin crystallinity"	CSIRO
		KC_NoSM_22D+216DM_3MeFi.tif		CSIRO
	TXT_AMS/	2320D_vegunm.txt	AMS product "2320D", vegetation unmixed	CSIRO
		AlOHAbVegunm.txt	AMS product "Al-clay abundance index", vegetation unmixed	CSIRO
		FeOxVegUnm.txt	AMS product "Ferric Oxide Abundance Index", vegetation unmixed	CSIRO
		SRTM_RockleaDome+HardeyRiver.txt	Digital elevation model	GSWA

14

Rocklea Dome exercise	StudentExercises_Rocklea.docx	Exercises for analysis of HyLogging data	CSIRO
	Answers_CIDexercises.docx	Suggested answers to exercises for analysis of HyLogging data	CSIRO
	MinSpec_Workshop_7RockleaDomeTSG_HandsOn.pptx	PPT-presentation summarising Rocklea Dome exercise and results	CSIRO

269

270   The following chapters briefly describe examples of how the provided hyperspectral

271   and geochemical proximal and remote sensing data sets can be used to address challenges for

272   the mineral resources sector.

273

274   *5.1.   Drill core mineralogy and geochemistry*

275   Reflectance spectra collected from rock chips (RC) and diamond drill cores (RKD)

276   using CSIRO's HyChips™ system presented a cost-effective way to spatially map the major

277   ore (i.e. goethite +/- hematite) and gangue minerals (i.e. kaolinite, smectite, carbonate), apart

278   from quartz, in detail. To achieve this, the relative intensity of mineral-diagnostic absorption

279   features was calculated using a suite of batch scripts ("Geoscience Products" in Haest et al.,

280   2012a). The relative intensity of the respective absorption features correlates with the relative

281   abundance of the respective mineral, whereas the wavelength position of key absorption

282   features relates to mineral speciation (e.g. ochreous versus vitreous goethite) or determining

283   the mineral chemistry. For example, the relative abundance of iron oxides was calculated from

284   the relative depth of the ferric iron-related absorption at around 900 nm (Cudahy &

285   Ramanaidou, 1997), whereas goethite was distinguished from hematite by tracking the

286   wavelength position of the same absorption feature (Table 2 in Haest et al., 2012a).

287   Whole rock geochemistry obtained from the same drill core material showed significant

288   correlations with the Geoscience Products. Haest et al. (2012) determined an RMSE of 9.1

289   weight % Fe for the correlation between the hyperspectrally-derived iron oxide abundance and

290   the XRF weight % Fe data and an RMSE of 3.9 weight % Al_2O_3 for correlation between the

291 hyperspectrally-derived Al-clay abundance and the XRF weight % Al_2O_3 data. The errors

292 associated with the correlations were found to be due to a combination of grain size variations

293 and the transopaque behaviour of iron oxides and/or different amounts of silica, causing

294 variations in the optical depth of sample material.

295

296 *5.2.   Surface mineral mapping*

297 Airborne hyperspectral surveys provide spatially contiguous mineralogical information

298 of the Earth's surface at high spatial resolution (down to circa 1 m). The relative intensity of

299 mineral diagnostic absorption features and their wavelength positions can be used to infer the

300 relative abundance of the respective minerals and even variations of single mineral species in

301 terms of their cation composition, crystallinity and hydroxylation. The Rocklea Dome case

302 study data set was used by Haest et al. (2013) to demonstrate how quantitative mineral maps

303 can be produced by validation of airborne hyperspectral data against field data, including

304 reflectance spectra and XRF data collected from surface samples. The effect of both green and

305 dry vegetation cover was unmixed at the pixel-level using the Normalised Difference

306 Vegetation Index (NDVI; e.g. Tucker, 1979) and the continuum-removed depth of the

307 cellulose-lignin absorption centred at around 2,100 nm, respectively. The resulting mineral

308 mapping products have a higher spatial continuity, as well as higher accuracy of, for example,

309 mineral abundance or composition values shown in single pixels. This proved to be especially

310 useful in areas with outcropping CID, which appeared to be sub-economic from the original

311 iron oxide abundance mineral maps but showed as potentially economic CID resources when

312 the vegetation cover was unmixed (Figure 2).
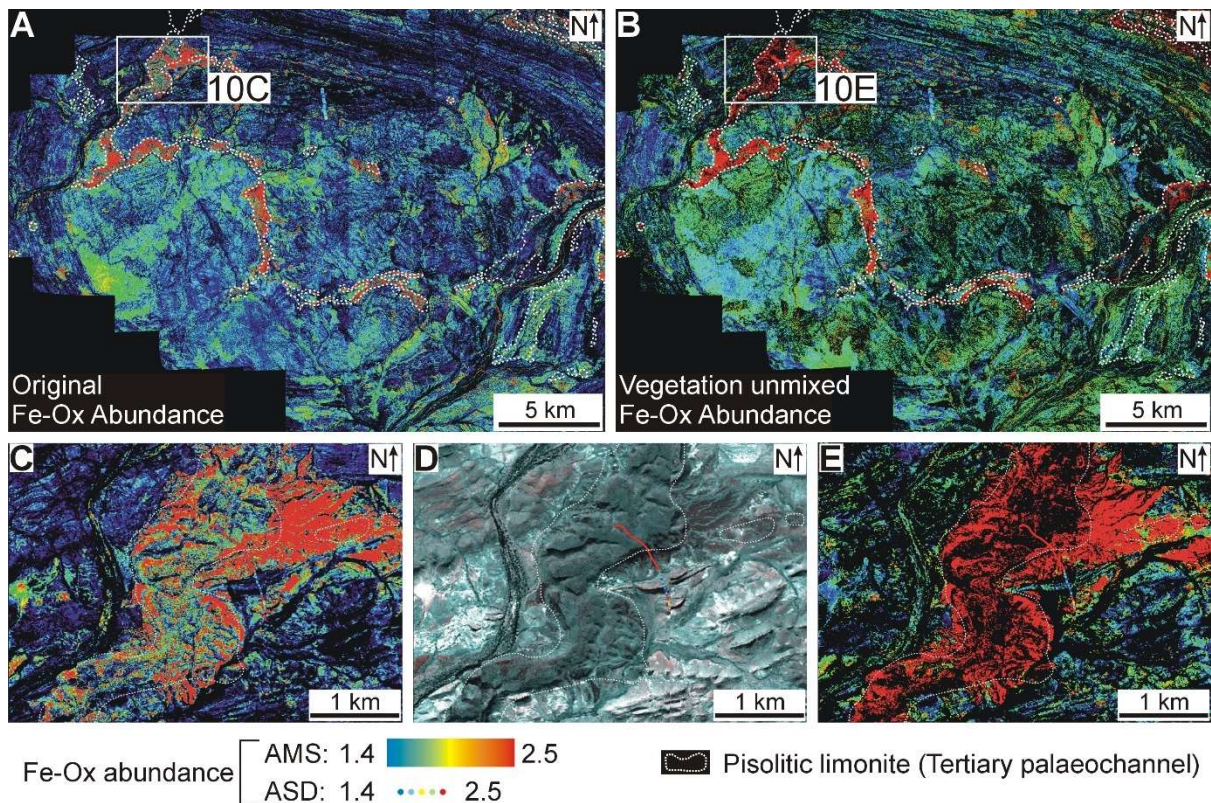
Figure 2: A–B: Fe-(oxyhydr-)oxide (Fe-Ox) abundance maps of the Rocklea Dome without (A) and with (B) vegetation unmixing. C–E: Fe-Ox abundance maps of the southern part of the Beasley River CID with (C) and without (E) vegetation removal and the false colour image of this area (D). The Beasley River CID has a plateau like surface expression, with the edges of the plateau clearly visible in the false colour image. These edges where mapped by the Geological Survey of Western Australia as representing the boundary of the pisolitic limonite (Fe-rich palaeochannel; white stippled line) (the Fe-Ox abundance measurements collected along transects 1 to 7 with the TerraSpec^{TM} are also shown for reference).

Beyond the iron oxide, kaolin and carbonate mineral maps published by Haest et al. (2013), airborne hyperspectral data can be used to create numerous additional mineral mapping products that can be used to address other geoscientific questions. For example, the Rocklea Dome presents a wide variety of igneous units that are part of the Proterozoic basement of the Pilbara Craton (Figure 1). These include 1) metamorphosed monzogranite, schist and chert, 2) metamorphosed basalt, and 3) amphibolite dykes. According to the white mica abundance derived from airborne hyperspectral data (green in Figure 3a), the metamorphosed monzogranite contains less white mica, when compared to the metamorphosed schists which

17

331 are striking East-West and occur in the northern part of the Rocklea Dome (red in Figure 3a).

332 In the eastern half of the Proterozoic basement in the Rocklea Dome, white mica is much less

333 abundant to absent. This coincides with elevated amounts of chlorite (folded lithologies in the

334 centre of Figure 3b), which map out metamorphosed basalt (Figure 1). The North-South

335 striking occurrence of chlorite in the Western half of the Proterozoic basement traces an

336 amphibolite dyke. Both the white mica abundance and chlorite abundance maps can also be

337 used to map out different lithologies in the metasediments and metabasalts of the Fortescue

338 that crop out to the North and South of investigated area, demonstrating how the airborne

339 hyperspectral data can be used to map out all major lithologies occurring in the Rocklea Dome

340 case study area.

341
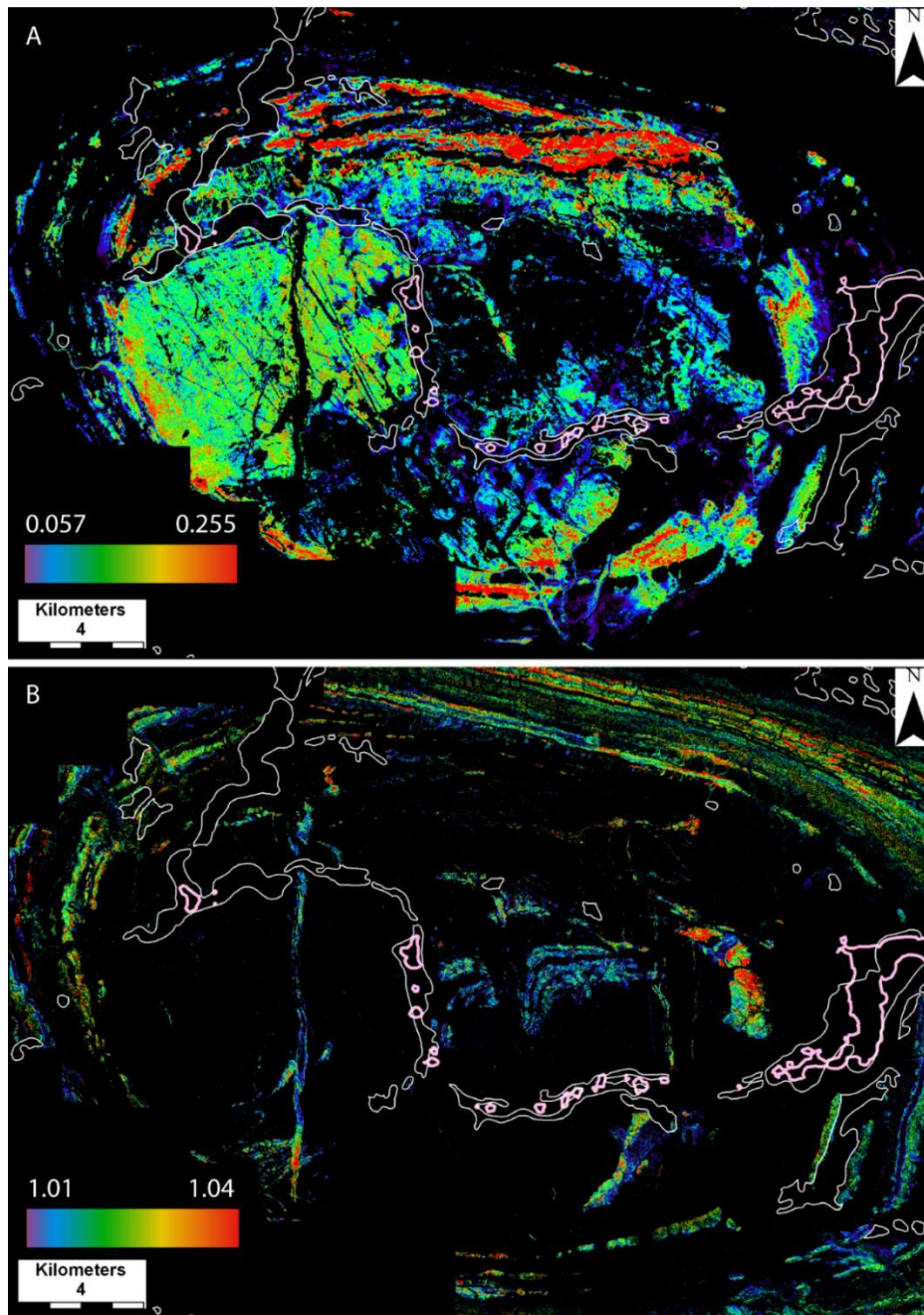
Figure 3: A & B: White mica (+Al-smectite) and chlorite (+epidote, +biotite) abundance
maps of the Rocklea Dome area in A and B, respectively, calculated from airborne
hyperspectral data using algorithms described in Table 1. Warm colours represent high
abundance and cool colours low abundance of the respective minerals. Black pixels have
been masked out as relative intensity of the absorption feature mapped in the respective
mineral map is below a given threshold (Table 1) and/or because of non-mineralogical effects
(e.g. vegetation, clouds). A shows monzogranites in the western part of the dome in green
colours and the Fortescue Group in the northern fringe of the dome in red colours. B
highlights Archean metamorphosed basalts in the eastern part of the dome structure and an N-
S trending amphibolite dyke in the western part of the dome. White lines indicate the surface
extension of the Tertiary paleochannel as mapped by Thorne & Tyler (1996). Pink lines

353 indicate the horizontal extension of the Tertiary paleochannel as mapped by the hyperspectral
354 data.

355

356 *5.3.   3D Mineral Mapping*

357   The hyperspectral drill core data can be combined with airborne hyperspectral data into

358 a seamless 3D mineral model of the Rocklea Dome CID (Figure 4). For this, all hyperspectral

359 data were resampled to the same spatial resolution and imported into the 3D modelling software

360 GoCad/SKUA^{TM}. The channel basement contact that was delineated at depth using the kaolin

361 crystallinity products could also be delineated at the surface from the airborne hyperspectral

362 image. A combination of both provided a seamless surface of the channel bottom (grey surface

363 in Figure 4) that separates the basement characterised by well-crystalline kaolinite from the

364 tertiary channel sediments characterised by poorly-crystalline kaolinite. The here identified

365 channel basement contact deviates at the surface significantly from the area mapped by the

366 geological survey as palaeochannel. This suggests that drilling patterns could have been much

367 better defined if the airborne hyperspectral-based surface outline would have been available

368 prior to drilling (Cudahy, 2016).

369   As part of their 3D Geomodel Series, the Geological Survey of Western Australia

370 (GSWA) provides access to 3D models of the Rocklea Dome area via their online portal:

371 https://dmpbookshop.eruditetechnologies.com.au/product/rocklea-inlier-2016-3d-geomodel-

372 series.do. The data can be viewed in three different formats (3D PDF, Geoscience Analyst,

373 GOCAD).

374
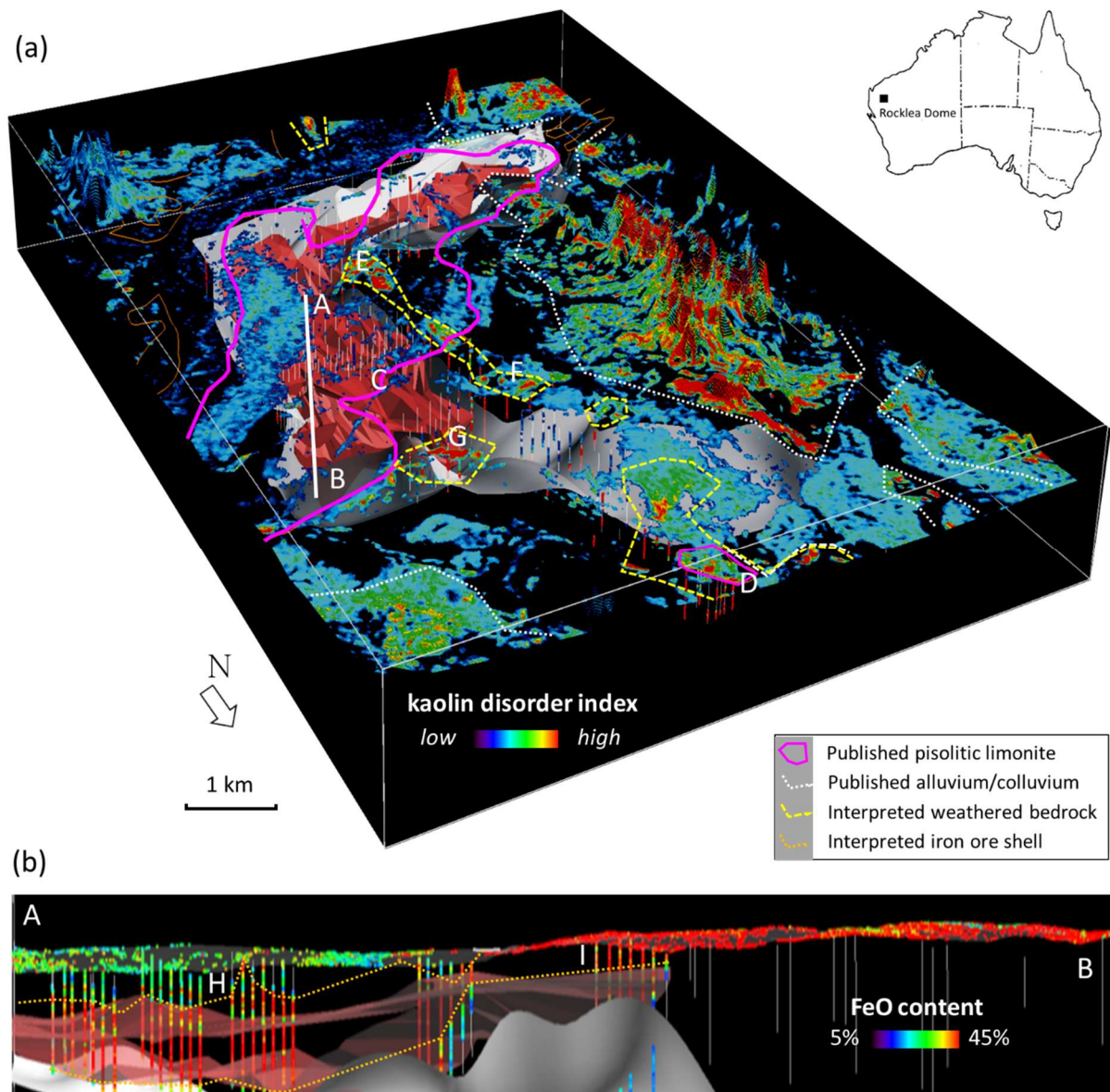
Figure 4: 3D mineral models of the Rocklea Dome area (Cudahy, 2016). Scene centre is approximately 22.8216° latitude 117.4652° longitude. (a) A southwest oblique 3D view of the Rocklea Dome study area showing kaolin disorder measured using airborne HyMap™ (surface) and drill core HyLogger™ (coloured vertical pegs) reflectance spectra. Warmer colours (well-ordered kaolin) relate to weathered, in situ bedrock, while cooler colours (poorly-ordered kaolin) relate to transported (alluvium/colluvium) materials. The interpolated model of the base of the channel iron system calculated using the 3D kaolin crystallinity map is shown by the shaded grey surface. The CID, which was calculated from the XRF-derived % FeO (Haest et al., 2012a), is shown by a shaded red volume (C). Areas of weathered bedrock (as mapped by Haest et al., 2012b; and Cudahy, 2016) are highlighted by yellow-coloured hashed lines and highlight which drill cores were sunk into barren ground (D, E, F, G). A white straight line shows the location of the cross-section (A–B) presented in (b); (b) Cross section A–B in (a) of the % FeO measured from the drill core and airborne imagery, which was vegetation unmixed (Haest et al., 2013). Orange, dotted polygon indicates the

21

390 shell of iron ore, which extends from under cover of ~20 m of alluvium (H) to exposed at the
391 surface (I).

392

393 *5.4.   Resource estimation*

394   Resource estimation of base and precious metal deposits requires the grouping of drill

395 hole data into domains that represent zones of homogenous properties for accurate grade

396 estimation and practical exploitation purposes. In practice, this is more than often performed

397 through a subjective time-consuming manual interpretation of sample analytical data.

398 Traditional automated clustering techniques, such as multivariate clustering and k-means, tend

399 to show poor spatial contiguity of domains in a mineral deposit. Fouedjio et al. (2017) used the

400 Rocklea Dome drill core data set to showcase how geostatistical clustering methods can take

401 spatial dependency into account (Figure 5). By integrating whole rock geochemistry and

402 hyperspectral drill core data, Fouedjio et al. (2017) revealed two distinct domains in the

403 Rocklea Dome Channel Iron Ore Deposit that are mainly characterised by four geochemical

404 variables (FeO, Al_2O_3, SiO_2 and TiO_2) and two mineralogical variables derived from

405 hyperspectral data (ferric oxide abundance and kaolinite abundance). Ore body domaining

406 through geostatistical clustering represents a method for objective samples clustering that

407 introduces scientific rigour to a traditionally subjective procedure. The robust domaining is

408 based in genuine multivariate geostatistics combining all available data. The flexible and

409 reproducible automatic domaining technique saves time, improves the understanding of

410 domains critical for exploitation of the ore and allows an easy integration of new data sets.

411

412
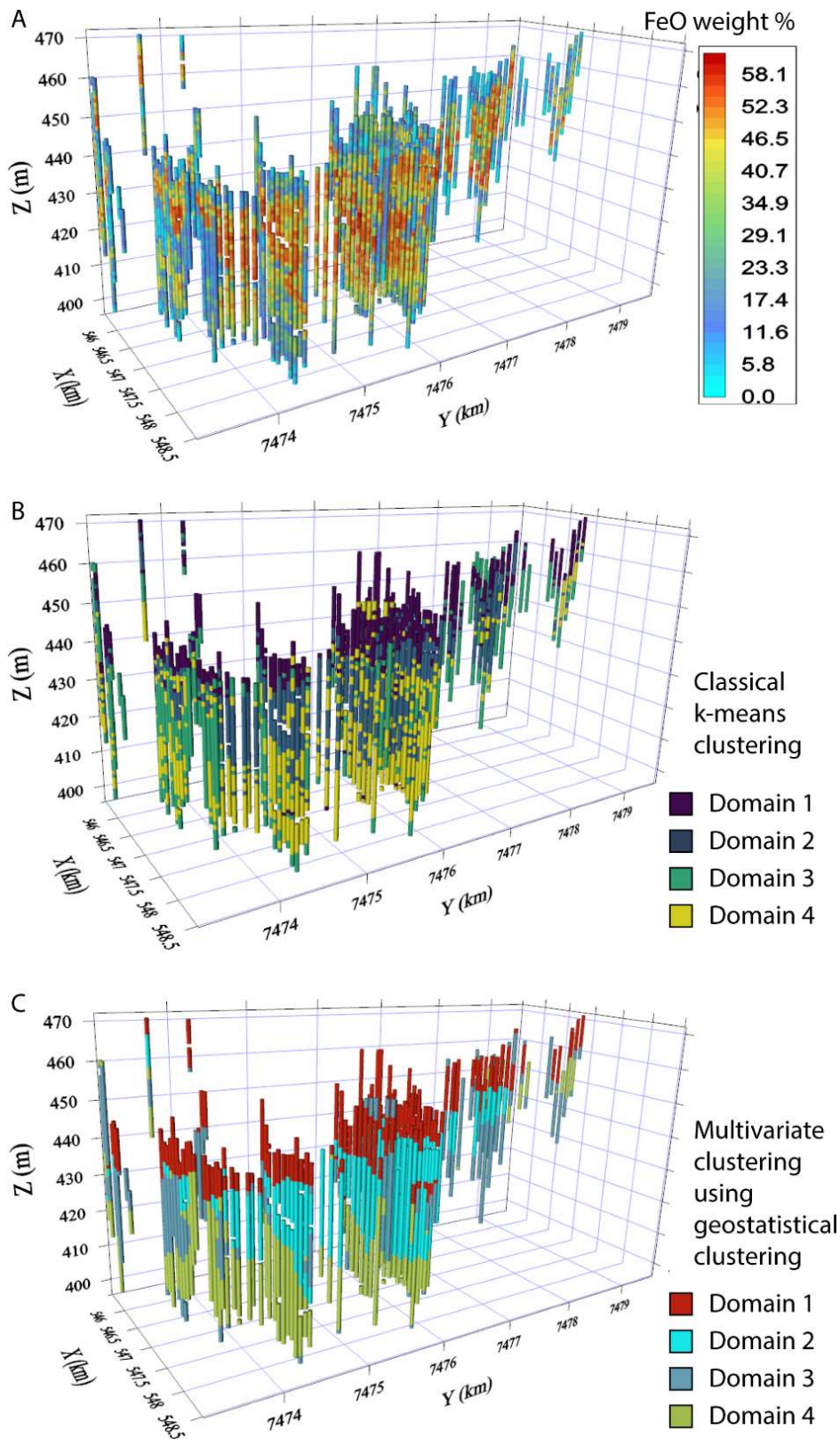
Figure 5: a) Spatial plot of FeO distribution in the Rocklea Dome Channel Iron Deposit. (b)
Classical k-means clustering method using 4 domains. (c) Geostatistical spectral clustering
using 4 domains. Z-axis was scaled to ease visualisation. Modified from Fouedjio et al.
(2017).

23

417

418

419

5.5.   Teaching material

The publicly available Rocklea Dome data set provided an opportunity to compile

training and teaching material about the application of hyperspectral drill core and chips data

for iron ore resource characterisation using The Spectral Geologist Software (TSG^{TM};

https://research.csiro.au/thespectralgeologist/). Student exercises and example answers, as well

as a ppt for teaching are part of the data package:

Exercise: StudentExercises_Rocklea.docx

Answers: Answers_CIDexercises.docx

PPT for teaching: MinSpec_Workshop_7RockleaDomeTSG_HandsOn.pptx

6. CONCLUSIONS AND OUTLOOK

We have established an open-access dataset comprising drill core, surface and airborne

hyperspectral data of the Rocklea Dome area in the Hamersley Basin of Western Australia,

which features a wide variety of lithologies and morphologies and is prospective for channel-

hosted iron ore resources. The proximal and remote sensing data, together with associated

whole rock geochemistry are ideal for researching the geology of this economically significant

area and allow a thorough comparison of different geoanalytical techniques and their

effectiveness for resource characterisation. Combining the surface and subsurface data into 3D

mineral maps provides a better visual understanding of the geological environment.

In addition to the already published surface and subsurface mineral mapping products,

many more Geoscience Products can be generated to better understand this geologically

complex area. The here newly presented white mica and chlorite abundance maps clearly

24

highlight the potential for mapping out different sections of the Archaean monzogranitic basement as well as different generations of mafic intrusives. Of particular interest are the contact zones between the mafic dykes and their host rocks, as they could help to better understand the intensity of alteration within the dyke and within the host granite as well as the associated fluid-rock interaction processes.

The teaching material provided together with this open-access dataset aims to support training of geoscience graduates and post-graduates in the potential applications of hyperspectral proximal and remote sensing data for mineral exploration and resource characterisation.

All analytical technologies used for collection of the geoscience data, as well as software packages used for processing the data, are commercially available. However, it should be noted that the HyChips™ system is now superseded by HyLogger3, which collects thermal infrared wavelengths (TIR; 6000 to 14500 nm) in addition to the VNIR-SWIR data. The collection of the TIR wavelength range enables the characterisation of major rock forming minerals such as quartz, which are of major importance for characterisation of iron ore resources, but were not detectable with HyChips™. The HyLogger3 technology is in operation at the six nodes of the Australian National Virtual Core Library (https://www.auscope.org.au/nvcl), which provides online open access to more than 3,500 drill cores from the Australian continent.

7. DATA AVAILABILITY

The supplement related to this article is available online at: https://doi.org/10.25919/5ed83bf55be6a (Laukamp, 2020). A 3D model of the Rocklea Dome data set is also available from the Geological Survey of Western Australia: https://dasc.dmp.wa.gov.au/DASC?productAlias=Rocklea3D.

8. AUTHOR CONTRIBUTIONS

CL, TC and MH contributed equally to the manuscript preparation. CL is the custodian of the Rocklea Dome data set stored on the CSIRO's Data Access Portal.

9. COMPETING INTERESTS

The authors declare that they have no conflict of interest.

REFERENCES

Berk, A., Anderson, G. P., Acharya, P. K., Bernstein, L. S., Muratov, L., Lee, J., et al. (2006). MODTRAN (TM) 5: 2006 update — art. no. 62331F. In S. S. L. P. E. Shen (Ed.), Algorithms

492   and technologies for multispectral, hyperspectral, and ultraspectral imagery, XII Pts 1 and 2. (pp.

493   F2331–F).

494 Berk, A., Cooley, T. W., Anderson, G. P., Acharya, P. K., Bernstein, L. S., Muratov, L., et al. (2004).

495   MODTRAN5: a reformulated atmospheric band model with auxiliary species and practical

496   multiple scattering options. In K. P. C. A. C. M. R. P. R. H. S. N. I. Schafer (Ed.), Remote sensing

497   of clouds and the atmosphere, Ix. (pp. 78–85).

498 Cocks, T., Jenssen, R., Stewart, A., Wilson, I., & Shields, T. (1998). The HyMap™ airborne

499   hyperspectral sensor: The system, calibration and performance. 1st EARSEL Workshop on

500   Imaging Spectroscopy, Zurich, October 1998 (http://www.neodc.rl.ac.uk/docs/

501   Hymap_specs.pdf)

502 Cudahy, T.J., 2016, Mineral Mapping for Exploration: An Australian Journey of Evolving Spectral

503   Sensing Technologies and Industry Collaboration. Geosciences 2016, 6, 52;

504   doi:10.3390/geosciences6040052

505 Cudahy, T.J., and Ramanaidou, E.R., 1997, Measurement of the hematite: goethite ratio using field

506   visible and near-infrared reflectance spectrometry in channel iron deposits, Western Australia:

507   Australian Journal of Earth Sciences, v. 44, p. 411−420.

508 Cudahy, T., Jones, M., Thomas, M., Laukamp, C., Caccetta, M., Hewson, R., Rodger, A., Verrall, M.

509   (2008): Next Generation Mineral Mapping: Queensland airborne HyMap and satellite ASTER

510   surveys 2006-2008.- CSIRO report P2007/364, 161pp.

511 Dean, W.E., 1974, Determination of carbonate and organic-matter in calcareous sediments and

512   sedimentary-rocks by loss on ignition—comparison with other methods: Journal of Sedimentary

513   Petrology, v. 44, p. 242−248.

514 Fouedjio, F., Hill, E.J., Laukamp, C. (2018): Ore Body Domaining through Geostatistical Clustering:

515   Case Study at the Rocklea Dome Channel Iron Ore Deposit, Western Australia.- Applied Earth

516   Science, Volume 127(1), 15-29.

517 Haest, M., Cudahy, C., Rodger, A., Laukamp, C., Martens, C., Caccetta, M. (2013): Unmixing

518   vegetation from airborne visible-near to shortwave infrared spectroscopy-based mineral maps

519   over the Rocklea Dome (Western Australia), with a focus on iron rich palaeochannels.- Remote

520   Sensing of Environment, 129, 17-31.

521   Haest, M., Cudahy, T., Laukamp, C., Gregory, S. (2012a): Quantitative mineralogy from visible to

522   shortwave infrared spectroscopic data - I. Validation of mineral abundance and composition

523   products of the Rocklea Dome channel iron deposit in Western Australia.- Economic Geology,

524   107, 209 - 228.

525   Haest, M., Cudahy, T., Laukamp, C., Gregory, S. (2012b): Quantitative mineralogy from visible to

526   shortwave infrared spectroscopic data - II. 3D mineralogical characterisation of the Rocklea

527   Dome channel iron deposit, Western Australia - Economic Geology, 107, 229 - 249.

528   Haest, M., Cudahy, T., Laukamp, C. (2012c): Application of infrared spectroscopy-based mineralogy

529   to channel iron ore resource evaluation.- Resource Evaluation and Mining 2012, 30.03.2012,

530   Perth, 29-33.

531   Huntington, J., Mauger, A., Skirrow, R., Bastrakov, E., Connor, P., Mason, P., Keeling, J., Coward, D.,

532   Berman, M., Phillips, R., Whitbourn, L., Heithersay, P., and AusIMM, 2004, Automated

533   mineralogical logging of core from the Emmie Bluff, iron oxide copper-gold prospect, south

534   Australia, Pacrim 2004 Congress, 2004: Parkville Victoria, Australasian Institute of Mining and

535   Metallurgy Publication Series, p. 223−230.

536   Laukamp, C., Cudahy, T., Caccetta, M., Chia, J., Gessner, K., Haest, M., Liu, Y.C., Rodger, A. (2010):

537   The uses, abuses and opportunities for hyperspectral technologies and derived geoscience

538   information.- AIG Bulletin, 51(Geo-Computing 2010 Conference, Brisbane, September 2010):

539   73-76.

540   Laukamp, C. (2011): Short Wave Infrared Functional Groups of Rock-forming Minerals.- CSIRO

541   report EP115222.

542   Laukamp,   C.   (2020):   Rocklea   Dome   C3DMM.   v1.   CSIRO.   Data   Collection.

543   https://doi.org/10.25919/5ed83bf55be6a

544   Morris, R. C., & Ramanaidou, E. R. (2007). Genesis of the channel iron deposits (CID) of the Pilbara

545   region, Western Australia. Australian Journal of Earth Sciences, 54, 733–756.

546 Ramanaidou, E.R., Morris, R.C., and Horwitz, R.C., 2003, Channel iron deposits of the Hamersley
547   Province, Western Australia: Australian Journal of Earth Sciences, v. 50, p. 669−690.

548 Rodger, A. (2011). SODA: A new method of in-scene atmospheric water vapor estimation and post-
549   flight spectral recalibration for hyperspectral sensors: Application to the HyMap sensor at two
550   locations. Remote Sensing of Environment, 115, 536–547.

551 Rodger, A. & Cudahy, T. (2009): Vegetation corrected continuum depths at 2.20 mm: An approach for
552   hyperspectral sensors.- Remote Sensing of Environment, 113: 2243-2257.

553 Sonntag, I., Laukamp, C., Hagemann, S. (2012): Low potassium hydrothermal alteration in low
554   sulfidation epithermal systems as detected by IRS and XRD: an example from the Co-O Mine,
555   Eastern Mindanao, Philippines.- Ore Geology Reviews, 45, 47-60.

556 Strezov, V., Ziolkowski, A., Evans, T.J., and Nelson, P.F., 2010, Assessment of evolution of loss on
557   ignition matter during heating of iron ores: Journal of Thermal Analysis and Calorimetry, v. 100,
558   p. 901−907.

559 Thorne, A.M., & Tyler, I.M. (1996). Geology of the Rocklea 1:100000 sheet. Perth: Western Australia
560   Geological Survey.

561 Tucker, C. J. (1979). Red and photographic infrared linear combinations for monitoring vegetation.
562   Remote Sensing of Environment, 8, 127–150.

563